This article has been accepted for publication in a future issue of this journal, but has not been fully edited. Content may change prior to final publication. Citation information: DOI 10.1109/LED.2017.2731859, IEEE Electron Device Letters

Linking Conductive Filament Properties and Evolution to Synaptic Behavior of RRAM Devices for Neuromorphic Applications

Jiyong Woo, Andrea Padovani, Kibong Moon, Myounghun Kwak, Luca Larcher, and Hyunsang Hwang

***Abstract*— We perform a comparative study of HfO_2 and Ta_2O_5 RRAM devices for their possible application as electronic synapses. By means of electrical characterization and simulations, we link their electrical behavior (digital or analog switching) to the properties and evolution of the conductive filament (CF). More specifically, we identify that bias-polarity-dependent digital switching in HfO_2 RRAM is primarily related to the creation and rupture of an oxide barrier. Conversely, the modulation of the CF size in Ta_2O_5 RRAM allows bias-polarity-independent analog switching with multiple states. Therefore, when the Ta_2O_5 RRAM is used to implement a synapse in multilayer perceptron neural networks operated by back-propagation algorithms, patterns in handwritten digits can be recognized with high accuracy.**

***Index terms*—Resistive switching memory (RRAM), filamentary switching, synaptic device, neuromorphic systems**

I. Introduction

Neuromorphic technology has recently demonstrated brain-inspired computing systems that can process massive amounts of data using low-power operations [1]. These systems are based on structures similar to the human brain, consisting of neurons connected by numerous synapses. They follow a simple weight update rule through synapses, similar to how humans remember information [2]. Different electronic devices are currently investigated for the development of artificial synapses, such as three-terminal transistor [1], phase change memory [3-4], spin-based memory [5], and resistive switching memory (RRAM) [6-11]. Among them, the RRAM based on filamentary switching is very promising owing to its excellent scalability, which enables the construction of large-scale neuromorphic systems.

In order for the RRAM to function as a synapse that can transfer weight in the form of either conductance or current, multiple current states that can be continuously increased (potentiation) or decreased (depression) using electrical signals are essential. Such states can be obtained by controlling the formation and rupture of the conductive filament (CF) in the RRAM. However, many studies have reported that only two discrete states are demonstrated during potentiation, whereas depression demonstrates multiple states [9-11]. This asymmetric synaptic characteristic degrades the pattern recognition accuracy in neuromorphic systems [3].

Manuscript received 23 June 2017. This research was supported by the MOTIE (10067794) and KSRC support program for the development of the future semiconductor device.

J. Woo, K. Moon, M. Kwak, and H. Hwang are with the Department of Materials Science and Engineering, Pohang University of Science and Technology, Pohang, 790-784, South Korea (e-mail: hwanghs@postech.ac.kr).

A. Padovani is with MDLab s.r.l., 42122, Reggio Emilia, Italy with MDLSoft Inc., 5201 Great America Parkway, Suite 320, Santa Clara, CA 95054, USA.

L. Larcher is with Dipartimento di Scienze e Metodi dell'Ingegneria, Universtita di Modena e Reggio Emilia, 41125, Reggio Emilia, Italy.

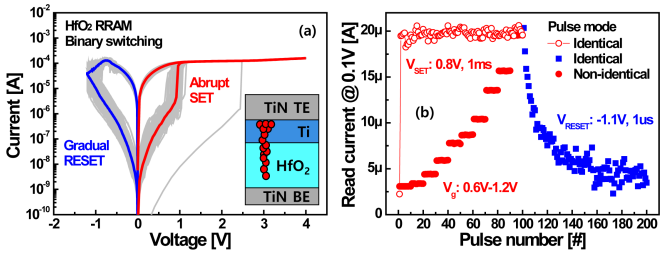

Fig. 1. (a) *I–V* characteristics for HfO_2 RRAM. The gray lines show 100 reliable switching cycles. Abruptly (or gradually) transited current states during SET (or RESET) indicated by bold red (or blue) lines are shown. (b) Binary and multiple states are shown by identical pulses at the fixed V_g during potentiation and depression, respectively. Whereas, varying V_g results in multiple states in potentiation at the fixed SET conditions.

In this study, we compare two different RRAM device stacks and use experiments and simulations to understand and explain their different behavior in terms of properties and evolution of the CF. Our findings shed some light on the physical mechanisms allowing achieving analog switching with multiple states required by RRAM synaptic devices.

II. Experiments

Two RRAM systems using HfO_2 and Ta_2O_5 as switching layers were utilized in this study. A 6-nm-thick HfO_2 layer was deposited on top of a 400-nm TiN bottom electrode (BE) connected to a 0.35 µm transistor. A 15-nm-thick Ti top electrode (TE) was then deposited, resulting in Ti TE/HfO_2/TiN BE stack [7]. Meanwhile, for the Ta_2O_5 RRAM, bilayered TiO_x/Ta_2O_5 was sandwiched between TiN BE/TE, where TiO_x served as an oxygen reservoir [12]. RRAM operations were simulated using the Ginestra™ software package that described self-consistently charge transport, power dissipation and temperature increase and oxygen ions/vacancies generation, diffusion, and recombination processes [13-14].

III. Results and Discussion

Fig. 1(a) shows the current-voltage (*I-V*) characteristics of an HfO_2 RRAM operated under 100 µA compliance current in 1T-1R configuration. During cycling the high-resistance state (HRS) was abruptly transited to a low-resistance state (LRS) during the SET operation. Then, the current of the LRS began

This article has been accepted for publication in a future issue of this journal, but has not been fully edited. Content may change prior to final publication. Citation information: DOI 10.1109/LED.2017.2731859, IEEE Electron Device Letters

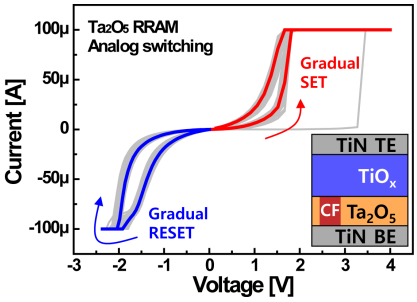

Fig. 2. *I–V* characteristics of Ta_2O_5 RRAM. 100 switching cycles are shown in gray lines. Gradually transited current states during SET and RESET indicated by bold red and blue lines are shown.

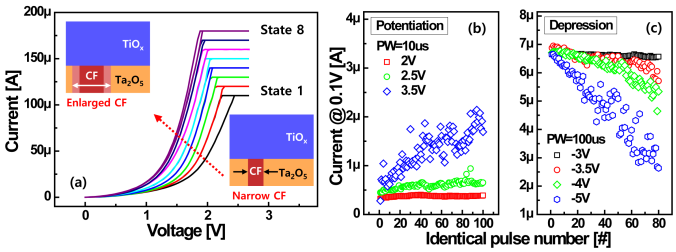

Fig. 3. (a) Continuously increasing current during potentiation by current ramping in the Ta_2O_5 RRAM. (b) and (c) Linearly modulated potentiation and depression behaviors as functions of the number of identical positive pulses of 2 to 3.5 V for 10 µs and negative pulses of −3 to −5 V for 100 µs.

to decrease gradually toward the HRS during the RESET operation. A similar bias-polarity-dependent switching behavior was observed when identical SET/RESET pulses with a fixed gate voltage (V_g) of 1.2 V were applied sequentially to the HfO_2 RRAM, as shown in Fig. 1(b). A sudden increase in the current is caused by the first positive pulse leading to a current saturation region. No further changes in the current are observed after subsequent pulses, resulting in binary states during potentiation. Instead, applying non-identical pulse that increases the transistor V_g from 0.6 to 1.2 V at the fixed SET voltage allowed proportionally increased read currents, which enabled the binary states to be divided into multiple states. During depression, the current began to decrease continuously, in accordance with the number of negative pulses.

On the other hand, the Ta_2O_5 RRAM exhibited bias-polarity-independent *I-V* curves, as shown in Fig. 2. After an abrupt forming process, analog switching corresponding to a gradual SET transition from the HRS to the LRS, and vice versa, was observed. Furthermore, we analyzed the current response by applying consecutive electrical inputs to the Ta_2O_5 RRAM. As can be seen in Fig. 3(a), the current increased continuously for a continuous increase in the compliance current. The current was thus tuned monotonically when 100 positive identical pulses between 2 and 3.5 V and 100 negative identical pulses between -3 and -5 V were applied for 10 µs and 100 µs, respectively, differently from the abrupt current jump exhibited by the HfO_2 RRAM under similar pulse operation, as shown in Figs. 3(b) and 3(c). The large amplitudes of the pulses showed high degrees of increase and decrease in the current change.

The results shown in Figs. 1 and 3 demonstrate that the binary and analog switching types depend on both the material system and on the way the RRAM cell is operated (compliance current modulation and identical pulse train), suggesting a strong connection with the properties and evolution of the CF in the RRAM system during switching. We used simulations to shed some light on these important aspects. First of all, we investigated how the read current (I_R) depends on the evolution of the CF considering two scenarios where the applied pulses are assumed to modulate either an oxide barrier (δ) or the CF size, as shown in Figs. 4(a) and 4(b), respectively. Simulations reveal that the CF current depends exponentially on the thickness of a large δ (> 1 nm) and linearly on the size of the CF (Fig. 4(b)). A linear current variation is also observed with the thickness of a small δ (< 1 nm); see state 'B' in Fig. 4(a).

We then simulated switching dynamics and pulsed operation in both HfO_2 and Ta_2O_5 based RRAM devices. RESET simulations of the HfO_2 device show the formation of a clear δ (~1.5-2 nm, Fig. 5(b)) that allows to nicely reproduce the measured HRS current (not shown for brevity). Based on the results in Fig. 4(a), the modulation of such a thick δ is expected to lead to an exponential variation of the current. This is consistent with the large jump of I_R observed during potentiation, Fig. 1(b), whose abrupt nature – determining the binary switching exhibited by HfO_2 devices – can be understood by looking at pulsed SET dynamics. Simulations reveal that when the train of identical SET pulses is applied, the voltage drops almost entirely across the δ, owing to the metallic-like nature of the remaining CF portion [14]. As a consequence, vacancies (V_0) are massively generated, quickly restoring the CF already within the first pulse, see Figs. 5(a) and (c). The electric field becomes thus lower and uniform across the restored CF, strongly reducing the probability to generate additional V_0 during the subsequent pulses and determining the observed saturation of the read current, Figs. 1(b) and 5(a). This also explains why subsequent pulses do not lead to an enlargement of the CF. Once the CF is recreated, the electric field is approximately equal to V_P/t_{OX} ~ 1.7 MV/cm (being t_{OX} the HfO_2 thickness), which is far lower than the critical field of ~ 4-5 MV/cm needed to break Hf-O bonds [15].

Simulations allow also to understand and explain the analog behavior exhibited by the Ta_2O_5 RRAM. Forming results show that the CF is created only in the thin Ta_2O_5, whereas the overlying TiO_x acts as a reservoir for the generated oxygen ions

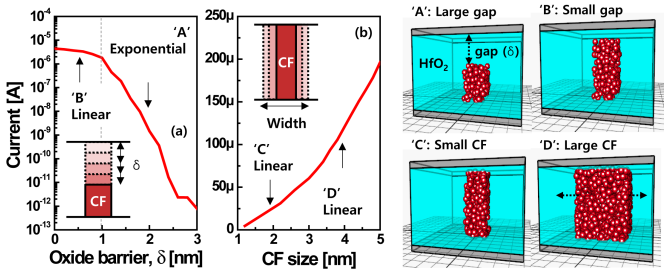

Fig. 4. Simulation results showing the current responses of CFs evolved by modulating either the δ or the size in the HfO_2 RRAM systems. (a) Change in the δ (> 1 nm) primarily induces an exponential current change, whereas a linear increase in the current is observed for an increase in the CF size (b).

This article has been accepted for publication in a future issue of this journal, but has not been fully edited. Content may change prior to final publication. Citation information: DOI 10.1109/LED.2017.2731859, IEEE Electron Device Letters

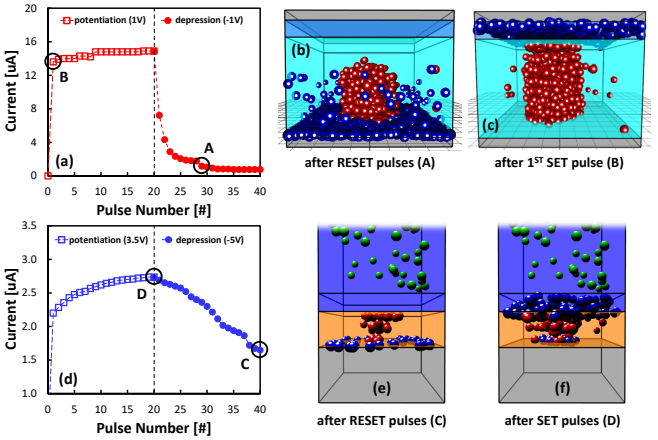

Fig. 5. The amplitude (V_P) and width (t_P) of the SET/RESET pulse applied to the experiment were used in the simulation. The read pulse of 0.12 V and width (t_R) was applied after the SET/RESET pulse. (a) I_R simulated during a sequence of 20 SET pulses (V_P=1 V, t_P=t_R=1 ms) and 20 RESET pulses (V_P=-1 V, t_P=1 μs, t_R=1 ms) applied to the HfO_2 device. (b)-(c) 3D maps of V_0 (red spheres) and O^- (blue spheres) distributions corresponding to the device states after the RESET pulses and after the 1st SET pulse (marked respectively as A and B in (a)). (d) I_R simulated during a sequence of 20 SET pulses (V_P=3.6 V, t_P=10 μs, t_R=100 μs) and 20 RESET pulses (V_P=-5 V, t_P=t_R=100 μs) applied to the Ta_2O_5 device. (e)-(f) 3D maps of V_0 (red spheres) and O^- (blue spheres) distributions corresponding to the device states after the RESET pulses and after the SET pulses (marked respectively as C, and D in (d)).

(O^-) [12], [16], Figs. 5(e)-(f). As expected, when applying the RESET voltage ramp or pulses, the O^- accumulated into the TiO_x diffuse back into the Ta_2O_5 under the action of the electric field. However, simulations reveal rather different process dynamics with respect to the case of the HfO_2 RRAM, which originates from the different properties of the TiO_x/Ta_2O_5 material system. In fact, oxygen diffusion in Ta_2O_5 is characterized by a larger activation energy (~1.2 eV [17]) and by a smaller field acceleration factor, respectively determining a slower and more *random* diffusion process (the reduced dependence on the applied field makes easier for O^- to move radially driven by the local temperature and mutual Coulomb repulsion [14]). These microscopic material-related aspects translate into a more gradual and uniform oxidation of the CF. Simulation results clearly show that the RESET operation leads to a modulation of the CF size rather than to the creation of the δ, see Fig. 5(e). This affects also the following pulsed SET operation. Since the electric field is relatively uniform across the remaining oxide (no barrier is formed), V_0 are generated preferentially in the surrounding of the CF (where the local temperature is higher [14]), determining its enlargement, Fig. 5(f). Therefore, the bias-polarity-independent analog switching behavior in the Ta_2O_5 RRAM is primarily related to the change in the width of the CF, and not on the abrupt CF reconstruction, in full agreement with the results in Fig. 4(b).

We finally simulated pattern recognition using the MNIST database of handwritten digits, for evaluating the operation of these RRAM devices as synapses in neural networks based on multilayer perceptron, which comprise input, hidden, and output layers, as shown in Fig. 6(a). Using a cropped 22 x 24 image as input, the number of input neurons (528) was defined [18]. The signals are transferred from the input neurons to the output neurons via the synapse weights. The synaptic weight

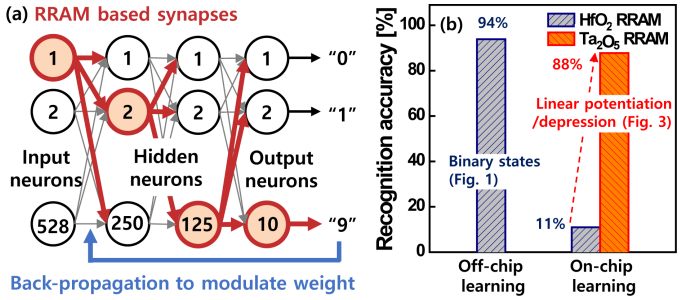

Fig. 6. (a) Schematic diagram of neural network based on multilayer perceptron. Pattern recognition in MNIST handwritten dataset is trained by back-propagation algorithm. (b) Using HfO_2 RRAM with binary states serving as synapse in the neural networks, the MNIST image can be recognized with 94% accuracy in off-chip learning; however, the binary states limit the improvement of recognition accuracy during on-chip learning. Thus, the use of a Ta_2O_5 RRAM capable of linearly increasing or decreasing multiple states improves the recognition accuracy.

was considered as the conductance difference in a pair of two RRAM devices and updated by the back-propagation algorithm [3]. We then examined the effect of linearity of the conductance change on recognition accuracy. In off-chip learning, where training was performed using software, pattern recognition with 94% accuracy was achieved by utilizing the binary states achieved from the HfO_2 RRAM based synapses, as shown in Fig. 6(b) [19]. During on-chip learning, however, the back-propagation algorithm repeatedly compared the output results and correct answers by adjusting the weight of the synapse to reduce the error rate of recognition [3]. In this case, the synapses with binary states had limitations in improving the recognition accuracy. The data could be recognized more precisely using the linearly modulated multiple states in the Ta_2O_5 RRAM based synapses in neuromorphic systems, thereby enabling improved accuracy (88%) of pattern recognition.

IV. Conclusion

We used experiments and simulations to perform a comparative study between HfO_2 and Ta_2O_5 RRAMs and revealed that the evolution and properties of the CF play a crucial role in determining device electrical behavior (digital or analog switching). In particular, switching in the TiO_x/Ta_2O_5 material system is obtained through a modulation of the CF size, which allows achieving analog switching suitable for electronic synapses. Our findings provide fundamental insights for the development of RRAM devices to be used for neuromorphic applications.

Acknowledgments

The authors would like to thank S. Kim of SK Hynix for fruitful discussion.

REFERENCES

[1] P. A. Merolla, J. V. Arthur, R. A. Icaza, A. S. Cassidy, J. Sawada, F. Akopyan, B. L. Jackson, N. Imam, C. Guo, Y. Nakamura, B. Brezzo, I. Vo, S. K. Esser, R. Appuswamy, B. Taba, A. Amir, M. D. Flickner, W. P. Risk, R. Manohar, D. S. Modham, "A million spiking-neuron integrated circuit with a scalable communication network and interface," *Science*, vol. 345, 6197, pp, 668-673, 2014. DOI: 10.1126/science.1254642

[2] C. Mead, "Neuromorphic electronic systems," *Proc. IEEE*, vol. 78, no. 10, pp. 1629-1636, Oct. 1990. DOI: 10.1109/5.58356

[3] G. W. Burr, R. M. Shelby, S. Sidler, C. Nolfo, J. Jang, I. Boybat, R. S. Shenoy, P. Narayanan, K. Virwani, E. U. Giacometti, B. N. Kurdi, and H. Hwang, "Experimental demonstration and tolerancing of a large-scale neural network (165000 synapses) using phase-change memory as the synaptic weight element," *IEEE Transactions on Electron Devices*, vol. 62, no. 11, pp. 3498-3507, 2015. DOI: 10.1109/TED.2015.2439635

[4] M. Suri, D. Querlioz, O. Bichler, G. Palma, E. Vianello, D. Vuillaume, C. Gamrat, and B. D. Salvo, "Bio-inspired stochastic computing using binary CBRAM synapses," *IEEE Transactions on Electron Devices*, vol. 60, no. 7, pp. 2402-2409, 2013. DOI: 10.1109/TED.2013.2263000

[5] A. F. Vincent, J. Larroque, N. Locatelli, N. B. Romdhane, O. Bichler, C. Gamrat, W. S. Zhao, J. O. Klein, S. G. Retailleau, and D. Querlioz, "Spin-transfer torque magnetic memory as a stochastic memristive synapse for neuromorphic system," *IEEE Transactions on Biomedical Circuits and Systems*, vol. 9, no. 2, pp. 166-174, 2015. DOI: 10.1109/TBCAS.2015.2414423

[6] S. Park, H. Kim, M. Choo, J. Noh, A. Sheri, S. Jung, K. Seo, J. Park, S. Kim, W. Lee, J. Shin, D. Lee, G. Choi, J. Woo, E. Cha, J. Jang, C. Park, M. Jeon, B. Lee, B. H. Lee, and H. Hwang, "RRAM-based synapse for neuromorphic system with pattern recognition function," *IEEE International Electron Devices Meeting*, 10.2.1-10.2.4, 2012. DOI: 10.1109/IEDM.2012.6479016

[7] J. Woo, K. Moon, J. Song, S. Lee, M. Kwak, J. Park, and H. Hwang, "Improved synaptic behavior under identical pulses using AlO_x/HfO_2 bilayer RRAM array for neuromorphic system," *IEEE Electron Device Letters*, vol. 37, no. 8, pp. 994-997, 2016. DOI: 10.1109/LED.2016.2582859

[8] J. Woo, K. Moon, J. Song, M. Kwaw, J. Park, and H. Hwang, "Optimized programming scheme enabling linear potentiation in filamentary HfO_2 RRAM synapse for neuromorphic systems," *IEEE Transactions on Electron Devices*, vol. 63, no. 12, pp. 5064-5067, 2016. DOI: 10.1109/TED.2016.2615648

[9] S. Ambrogio, S. Balatti, V. Milo, R. Carboni, Z.-Q. Wang, A. Calderoni, N. Ramaswamy, and D. Ielmini, "Neuromorphic learning and recognition with one-transistor-one-resistor synapses and bistable metal oxide RRAM," *IEEE Transactions on Electron Devices*, vol. 63, no. 4, pp. 1508-1515, 2016. DOI: 10.1109/TED.2016.2526647

[10] B. Gao, Y. Bi, H. Chen, R. Liu, P. Huang, B. Chen, L. Liu, X. Liu, S. Yu, H.-S. P. Wong, and J. Kang, "Ultra-low-energy three-dimensional oxide-based electronic synapses for implementation of robust high-accuracy neuromorphic computation systems," *ACS Nano*, vol. 8, no. 7, pp. 6998-7004, 2014. DOI: 10.1021/nn501824r

[11] S. Yu, B. Gao, Z. Fang, H. Yu, J. Kang, and H. –S. P. Wong, "A neuromorphic visual system using RRAM synaptic devices with sub-pJ energy and tolerance to variability: experimental characterization and large-scale modeling," *IEEE International Electron Devices Meeting*, 10.4.1-10.4.4, 2012. DOI: 10.1109/IEDM.2012.6479018

[12] H. Lee, S. G. Kim, K. Cho, H. Hwang, H. Choi, J. Lee, S. H. Lee, H. J. Lee, J. Suh, S.-O. Chung, Y. S. Kim, K. S. Kim, W. S. Nam, J. T. Cheong, J. T. Kim, S. Chae, E.-R. Hwang, S. N. Park, Y. S. Sohn, C. G. Lee, H. S. Shin, K. J. Lee, K. Hong, H. G. Jeong, K. M. Rho, Y. K. Kim, S. Chung, J.Nickel, J. J. Yang, H. S. Cho, F. Perner, R. S. Williams, J. H. Lee, S. K. Park, and S.-J. Hong, "Integration of $4F^2$ selector-less crossbar array 2Mb ReRAM based on transition metal oxides for high density memory applications," *Symposium on VLSI Technology*, pp. 151-152, 2012. DOI: 10.1109/VLSIT.2012.6242506

[13] MDLSoft Software: http://www.mdlsoft.com

[14] A. Padovani, L. Larcher, O. Pirrotta, L. Vandelli, and G. Bersuker, "Microscopic modeling of HfO_x RRAM operations: from forming to switching," *IEEE Transactions on Electron Devices*, vol. 62, no. 6, pp. 1998-2006, 2015. DOI: 10.1109/TED.2015.2418114

[15] M. Alayan, E. Vianello, B. De Salvo, L. Perniola, A. Padovani, and L. Larcher, "Correlated Effects on Forming and Retention of Al Doping in HfO_2-Based RRAM," *IEEE Design & Test*, vol. 34, no. 3, June 2017. DOI: 10.1109/MDAT.2017.2682246

[16] B. Kim, W. Kim, H. Kim, K. Jung, W. Park, B. Seo, M. Joo, K. Lee, K. Hong, and S. Park, "Low power and improved switching properties of selector-less Ta_2O_5 based resistive random access memory using Ti-rich TiN electrode," *Japanese Journal of Applied Physics*, 52, 04CD05, 2013. DOI: 10.7567/JJAP.52.04CD05

[17] R. Nakamura, T. Toda, S. Tsukui, M. Tane, M. Ishimaru, T. Suzuki, and H. Nakajima, "Diffusion of oxygen in amorphous Al_2O_3, Ta_2O_5, and Nb_2O_5," *Journal of Applied Physics*, vol. 113, pp. 033504, 2014. DOI: http://dx.doi.org/10.1063/1.4889800

[18] J. Jang, S. Park, G. W. Burr, H. Hwang, and Y. Jeong, "Optimization of conductance change in $Pr_{1-x}Ca_xMnO_3$-based synaptic devices for neuromorphic systems," *IEEE Electron Device Letters*, vol. 36, no. 5, pp. 457-459, 2015. DOI: 10.1109/LED.2015.2418342

[19] S. Yu, Z. Li, P. Chen, H. Wu, B. Gao, D. Wang, W. Wu, and H. Qian, "Binary neural network with 16 Mb RRAM macro chip for classification and online training," *IEEE International Electron Devices Meeting*, 16.2.1-16.2.4, 2016. DOI: 10.1109/IEDM.2016.7838429